



ChemComm

**Single-molecule magnet properties of a monometallic  
dysprosium pentalene complex**

Journal:	<i>ChemComm</i>
Manuscript ID	CC-COM-05-2018-003516.R1
Article Type:	Communication

SCHOLARONE™  
Manuscripts



Chem Comm

## COMMUNICATION

## Single-molecule magnet properties of a monometallic dysprosium pentalene complex

Received 00th January 20xx,  
Accepted 00th January 20xxAlexander F. R. Kilpatrick,<sup>a</sup> Fu-Sheng Guo,<sup>b</sup> Benjamin M. Day,<sup>b</sup> Akseli Mansikkamäki,<sup>\*c</sup>

DOI: 10.1039/x0xx00000x

Richard A. Layfield<sup>\*a</sup> and F. Geoffrey N. Cloke<sup>\*a</sup>

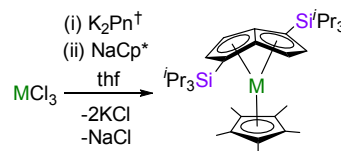
www.rsc.org/

The pentalene-ligated dysprosium complex  $[(\eta^8\text{-Pn}^\dagger)\text{Dy}(\text{Cp}^*)]$  (**1<sub>Dy</sub>**) ( $\text{Pn}^\dagger = [1,4\text{-}(\text{Pr}_3\text{Si})_2\text{C}_8\text{H}_4]^{2-}$ ) and its magnetically dilute analogue are single-molecule magnets, with energy barriers of  $245\text{ cm}^{-1}$ . Whilst the  $[\text{Cp}^*]^-$  ligand in **1<sub>Dy</sub>** provides a strong axial crystal field, the overall axiality of this system is attenuated by the unusual folded structure of the  $[\text{Pn}^\dagger]^{2-}$  ligand.

Single-molecule magnets (SMMs) are coordination compounds that display a magnetic memory effect and an effective energy barrier ( $U_{\text{eff}}$ ) to flipping of their magnetic dipoles.<sup>1</sup> Such materials have, thus far, proven to be of significant fundamental interest, however some SMMs have been incorporated into nanoscale molecular spintronic devices.<sup>2</sup> Ligand design continues to be a key strategy for addressing the properties of SMMs, particularly increasing the temperature at which slow magnetic relaxation can be observed. Synthetic approaches to the design of d- and f-block SMMs are dominated by Werner-type coordination chemistry,<sup>3</sup> however the organometallic approach to SMMs has led to some eye-catching recent examples.<sup>4,5</sup> Within the context of lanthanide SMMs, well-known organometallic ligands such as cyclopentadienide,  $[\text{Cp}]^-$ ,<sup>6,7</sup> cyclooctatetraenide,  $[\text{COT}]^{2-}$ ,<sup>8</sup> and cycloheptatrienide,  $[\text{C}_7\text{H}_7]^{3-}$ ,<sup>9</sup> have been used to influence the properties of dysprosium- and erbium-containing SMMs. In several notable examples, theoretical studies have provided detailed insight into how the properties of these organometallic ligands impact upon the electronic structure of the  $\text{Ln}^{3+}$  cation, leading to striking increases in the magnetic blocking temperature ( $T_B$ ) and  $U_{\text{eff}}$ .

In light of the advances made to date using organometallic chemistry, considerable scope remains for exploring other non-classical ligands in the context of single-molecule

magnetism, hence we now turn our attention to the dianion of pentalene, i.e.  $[\text{C}_8\text{H}_6]^{2-}$  or  $[\text{Pn}]^{2-}$ , an aromatic bicyclic ligand consisting of two fused  $\text{C}_5$  rings. Pentalene coordination chemistry<sup>10</sup> is considerably underdeveloped relative to that of more established  $\pi$ -organometallic ligands such as cyclopentadienide. However, important developments in the synthesis of pentalene pro-ligands have enabled the study of many pentalene complexes, which, in addition to the fundamental interest in their chemistry, have applications in catalysis and small-molecule activation,<sup>11</sup> and as models for metal-containing polymers.<sup>12</sup> When considered in the context of SMM design, pentalene offers a potential complement to cyclopentadienide and cyclooctatetraenide, the electronic structures of which are regarded as providing axial and equatorial crystal fields, respectively, suitable for slow magnetic relaxation based on dysprosium or erbium, respectively.<sup>6-8</sup> In particular, the formal dianionic charge and the  $\eta^8$ -coordination mode of pentalene, combined with the fold angle between the two fused rings,<sup>10</sup> provide a unique platform on which to construct new magnetic materials. We now describe the SMM properties of  $[(\eta^8\text{-Pn}^\dagger)\text{Dy}(\text{Cp}^*)]$  (**1<sub>Dy</sub>**) ( $\text{Pn}^\dagger = [1,4\text{-}(\text{Pr}_3\text{Si})_2\text{C}_8\text{H}_4]^{2-}$ ) and its magnetically dilute analogue, which were synthesized according to Scheme 1.

Scheme 1. Synthesis of **1<sub>M</sub>** with M = Y, Dy.

The addition of one stoichiometric equivalent of  $\text{K}_2\text{Pn}^\dagger$  to  $\text{MCl}_3$  ( $\text{M} = \text{Y}, \text{Dy}$ ) in thf, followed by one equivalent of  $\text{NaCp}^*$ , produced orange solutions from which crystals of **1<sub>Dy</sub>** and **1<sub>Y</sub>** were isolated in yields of 35% and 30%, respectively. X-ray crystallography confirmed the expected isostructural nature of **1<sub>Dy</sub>** (Fig. 1) and **1<sub>Y</sub>** (Fig. S4) (Tables S1, S2), with the metal centres being bound to an  $\eta^8\text{-Pn}^\dagger$  ligand and an  $\eta^5\text{-Cp}^*$  ligand.

<sup>a</sup> Department of Chemistry, School of Life Sciences, University of Sussex, Brighton, BN1 9QJ, UK. E-mail: F.G.Cloke@sussex.ac.uk, R.Layfield@sussex.ac.uk

<sup>b</sup> School of Chemistry, The University of Manchester, Manchester, M13 9PL, UK.

<sup>c</sup> Department of Chemistry, Nanoscience Center, University of Jyväskylä, P.O. Box 35, Jyväskylä, FI-40014, Finland. E-mail: akseli.mansikkamaki@jyu.fi

†Electronic Supplementary Information (ESI) available: Synthetic details, spectroscopic characterization, X-ray crystallography details and crystallographic information files, computational details. See DOI: 10.1039/x0xx00000x

The Dy-Pn<sub>cent</sub> distances of 2.235(3) Å are significantly shorter than the analogous Cp<sub>cent</sub> distance of 2.344(5) Å ('cent' denotes the centroid of a C<sub>5</sub> ring). The Dy–C distances to the

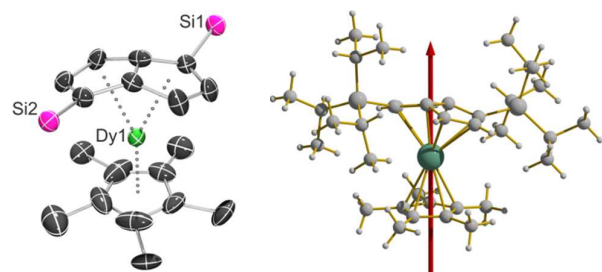


**Fig. 1** Left: Thermal ellipsoid representation (50% probability) of the molecular structure of **1<sub>Dy</sub>** (with H-atoms and <sup>1</sup>Pr groups omitted for clarity). Right: the principal axis of the g-tensor in the ground Kramers doublet of **1<sub>Dy</sub>**.

pentalene bridgehead carbon atoms C(4) and C(5) are 2.359(7) Å and 2.371(7) Å, whereas the distances to the wingtip carbons C(2) and C(7) are considerably longer at 2.749(6) Å and 2.731(6) Å, respectively. The Dy–C distances to the carbon atoms in the intermediate positions lie in the range 2.600(6)–2.640(6) Å and the pentalene fold angle is 26.9(4)° (Fig. S5). The range of Dy–C distances to the Cp\* ligand is 2.610(9)–2.643(12) Å (average 2.62 Å). **The two Pn<sub>cent</sub>–Dy–Cp<sub>cent</sub> angles are 152.47(11)° and 153.05(11)°.** The dysprosium centre in **1<sub>Dy</sub>** resides 0.200(2) Å above the plane of the three centroids, resulting in a pyramidal coordination environment with approximate C<sub>s</sub> symmetry. The shortest intermolecular Dy...Dy distance is 8.8313(8) Å. The solid-state molecular structures of **1<sub>Dy</sub>** and **1<sub>Y</sub>** are also consistent with the solution-phase structure of diamagnetic **1<sub>Y</sub>**, as confirmed by <sup>1</sup>H, <sup>13</sup>C and <sup>29</sup>Si NMR spectroscopy (Fig. S1–S3).

The magnetic properties of **1<sub>Dy</sub>**, which were measured in a static (D.C.) field of 5000 Oe, are typical of a monometallic Dy<sup>3+</sup> complex with a <sup>6</sup>H<sub>15/2</sub> ground term. Thus, the value of χ<sub>M</sub>T, where χ<sub>M</sub> is the molar magnetic susceptibility, is 13.51 cm<sup>3</sup> K mol<sup>−1</sup> at 300 K (Fig. S6), which is close to theoretical value of 14.17 cm<sup>3</sup> K mol<sup>−1</sup>. A gradual decrease in χ<sub>M</sub>T was observed down to about 20 K, at which point a precipitous drop occurred and a value of 7.60 cm<sup>3</sup> K mol<sup>−1</sup> was reached at 2 K. The overall temperature dependence of the susceptibility is indicative of depopulation of higher-lying crystal field states of Dy<sup>3+</sup> as the temperature is lowered, followed by the onset of magnetic blocking at very low temperatures. At 1.8 K and 5 K, the magnetization (*M*) of **1<sub>Dy</sub>** increases rapidly up to fields of about 10 kOe, followed by a more gradual increase at higher fields and reaching values of 5.0 μ<sub>B</sub> at 70 kOe (Fig. S6).

The SMM properties of **1<sub>Dy</sub>** were revealed through measurements of the in-phase (χ') and out-of-phase (χ'') A.C. magnetic susceptibility as a function of frequency (ν) (Figs 2 and S7). The χ''(ν) plot shows a series of well-defined maxima in the temperature range 2–41 K, with the position of the maxima shifting to higher frequencies as the temperature is raised. Cole-Cole plots of χ''(χ') in the same temperature range produced parabola-shaped curves, and fitting of the data with

a generalized Debye model yielded α parameters of 0.02–0.22, indicating a narrow distribution of relaxation times. Relaxation times, τ, were extracted from the A.C. susceptibility data and plotted as a function of T<sup>−1</sup> (Fig. 3), and the data were fitted according to equation 1:

$$\tau^{-1} = \tau_0^{-1} e^{-U_{\text{eff}}/k_B T} + C T^n + \tau_{\text{QTM}}^{-1} \quad (1)$$

In equation 1, τ<sub>0</sub><sup>−1</sup> and U<sub>eff</sub> denote the Orbach parameters, *C* and *n* denote the Raman parameters, and τ<sub>QTM</sub><sup>−1</sup> is the rate of quantum tunnelling of the magnetization (QTM). The following parameters were extracted for **1<sub>Dy</sub>**: U<sub>eff</sub> = 188(11) cm<sup>−1</sup>, τ<sub>0</sub> = 2.11 × 10<sup>−7</sup> s, *C* = 0.134 s<sup>−1</sup> K<sup>−*n*</sup>, *n* = 2.74 and τ<sub>QTM</sub> = 71.07 s. The same analysis on a 5% magnetically dilute sample of **1<sub>Dy</sub>**,

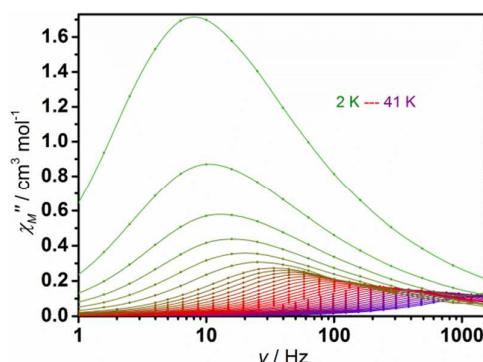


**Fig. 2** Frequency dependence of χ'' in zero applied field for **1<sub>Dy</sub>**. The solid lines are a guide for the eye.

i.e. **Dy@1<sub>Y</sub>** produced α parameters of 0–0.39 and U<sub>eff</sub> = 245(28) cm<sup>−1</sup>, τ<sub>0</sub> = 4.14 × 10<sup>−8</sup> s, *C* = 0.00639 s<sup>−1</sup> K<sup>−*n*</sup>, *n* = 3.62 and τ<sub>QTM</sub> = 4.63 s. **The apparent increase in the barrier of approximately 60 cm<sup>−1</sup> upon dilution implies that the contribution of Raman processes for 1<sub>Dy</sub> cannot be neglected even at high temperatures.** Re-fitting the relaxation dynamics of **1<sub>Dy</sub>** by fixing the energy barrier obtained for **Dy@1<sub>Y</sub>** gives, for **1<sub>Dy</sub>**, U<sub>eff</sub> = 245 cm<sup>−1</sup>, τ<sub>0</sub> = 2.94 × 10<sup>−8</sup> s, *C* = 0.05748 s<sup>−1</sup> K<sup>−*n*</sup>, *n* = 3.03 and τ<sub>QTM</sub> = 75.3 s.

Magnetic hysteresis in **1<sub>Dy</sub>** was observed by measuring the field-dependence of the magnetization with a sweep rate of

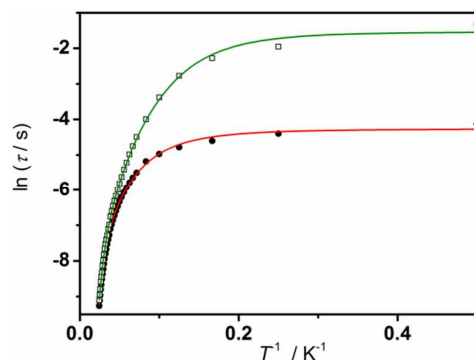


**Fig. 3** Temperature dependence of τ for **1<sub>Dy</sub>** (circles) and **Dy@1<sub>Y</sub>** (squares). Solid red lines represent fits of the data using the parameters stated in the text.

6.6 Oe s<sup>-1</sup>. Waist-restricted hysteresis loops were observed up to 2.4 K, although without any coercivity owing to prominent QTM processes. Similar measurements on **Dy@1<sub>y</sub>** allowed wider loops with small (e.g. 100 Oe at 1.8 K) coercive fields to be observed up to 3.0 K, which is consistent with the reduced significance of QTM in the diluted sample.

To provide further insight into the magnetic properties, the electronic structure of **1<sub>Dy</sub>** was studied by multi-reference *ab initio* calculations.<sup>13</sup> The coordinates of the heavy atoms were used in the calculations as determined by X-ray crystallography, and the positions of H atoms were optimized at the DFT level (see ESI for details). The experimental and calculated  $\chi_M T(T)$  agree well (Fig. S6), with the calculated  $\chi_M T$  value at 300 K being 13.80 cm<sup>3</sup> mol<sup>-1</sup> K, compared to the experimental value of 13.51 cm<sup>3</sup> mol<sup>-1</sup> K. The deviation is not large (~2%) and most likely results from neglecting electron correlation outside the 4f orbital space in the CASSCF calculations. The most important qualitative feature of the plot, namely, the gradual decrease in  $\chi_M T$  upon decreasing the temperature, is correctly produced. The calculated  $M(H)$  plots are in very good agreement with experiment (Fig. S6).

The energies of the eight lowest Kramers' doublets within the ground <sup>6</sup>H<sub>15/2</sub> multiplet of **1<sub>Dy</sub>**, along with the principal components of the respective *g*-tensors and the angles between the ground and excited doublets are listed in Table S3. The principal magnetic axis of the ground doublet in **1<sub>Dy</sub>** passes through the centre of the Cp\* ligand and the midpoint of the fused pentalene C–C bond (Fig. 1). The ground doublet is almost axial, with a large *g<sub>z</sub>* component and small transverse components, hence the QTM is completely blocked in the ground doublet. The angles between the magnetic axes of the ground doublet and the first three excited doublets are small, and then quickly become perpendicular in the higher doublets. The first excited doublet lies at 197 cm<sup>-1</sup>, which is quite close to the experimentally observed barrier height of 188 cm<sup>-1</sup> in **1<sub>Dy</sub>**. In the first excited state, the transverse components of the *g* tensor are still small, but not vanishingly so, and the QTM process is not completely blocked. Based on the experimental evidence, the QTM in this doublet is significant enough such that thermally activated QTM via the first excited doublet is the dominant relaxation mechanism.

The splitting of the <sup>6</sup>H<sub>15/2</sub> multiplets in **1** was studied further by calculating the *ab initio* crystal field (CF) parameters,<sup>14</sup> which are listed in Table S4. The decomposition of the SO-RASSI wave-functions of the sixteen lowest states (eight lowest doublets) into squared projections onto  $|JM_J\rangle$  states (where *J* = 15/2) is given in Table S5. The states in the lowest doublet have large squared projections (0.925) on the *M<sub>J</sub>* = ±15/2 states, as is usual for Dy<sup>3+</sup> SMMs.<sup>6,7</sup> The *M<sub>J</sub>* states become increasingly mixed as one moves to higher doublets. The first excited doublet has a squared projection of 0.888 on the *M<sub>J</sub>* = ±13/2 state and therefore still approximates to the *M<sub>J</sub>* = ±13/2 states. In higher doublets the correspondence of the SO-RASSI states with a single given *M<sub>J</sub>* state is lost.

The mechanisms for the relaxation of magnetization in **1<sub>Dy</sub>** was studied by constructing the qualitative relaxation barrier using a previously proposed method.<sup>15</sup> Plotting the energies of

the lowest states against their respective magnetic moments, with the states being connected by their transition magnetic moment matrix elements, provides the relaxation route corresponding to a pathway traced by the largest matrix elements. The resulting plot (Fig. 4) retains its “barrier-like” structure up to the sixth doublet. Based on the calculations, the most probable relaxation route in **1<sub>Dy</sub>** is an Orbach mechanism via the third excited Kramers doublet at 498 cm<sup>-1</sup>. However, the experimental data for **1<sub>Dy</sub>** show that the relaxation takes place via the first excited doublet. The QTM in this doublet is weak (roughly an order of magnitude stronger than in the ground doublet), but strong enough to overcome the Orbach route.

The anisotropy barriers and hysteresis properties determined for **1<sub>Dy</sub>** and **Dy@1<sub>y</sub>** are reminiscent of those found in the series of dysprosium metallocene SMMs reported by some of us,<sup>6,7a</sup> which have very similar Dy–C(Cp) distances to **1<sub>Dy</sub>**. Since Cp ligands in axial positions are known to promote SMM properties in complexes of Dy<sup>3+</sup>, the bridgehead pentalene carbon atoms, which occupy axial positions and are much closer to the metal centre, should also enhance the magnetic axiality. However, it is noticeable that the other Dy–C(Pn) distances – and the positions of the carbon atoms with respect to the metal centre – are similar to those found in dysprosium complexes of the [COT]<sup>2-</sup> ligand. Since [COT]<sup>2-</sup> is thought to diminish the magnetic axiality of the prolate Dy<sup>3+</sup> ion in, e.g., [Dy(COT)<sub>2</sub>]<sup>-</sup>,<sup>8</sup> we can propose that the non-bridgehead pentalene carbons in **1<sub>Dy</sub>** provide a non-negligible equatorial field and therefore produce an effect similar, yet stronger, to that of COT. Furthermore, the Pn<sub>cent</sub>–Dy–Cp<sub>cent</sub> in **1<sub>Dy</sub>** angles are 152.47(11)° and 153.05(11)°, hence they are very similar to the Cp–Dy–Cp angle of 152.845(2)° in [(Cp<sup>ttt</sup>)<sub>2</sub>Dy]<sup>+</sup>, an SMM with a barrier of 1277 cm<sup>-1</sup> and a *T<sub>B</sub>* of 60 K.<sup>7a</sup> Since the properties of [(Cp<sup>ttt</sup>)<sub>2</sub>Dy]<sup>+</sup> arise from the exceptional axiality of the ligand environment, the two opposing C<sub>5</sub> rings in the pentalene ligand of **1<sub>Dy</sub>** effectively compete with each other in a way that diminishes the axiality. Hence, **1<sub>Dy</sub>** is an SMM but with a modest barrier and waist-restricted hysteresis. The large, non-axial *B<sub>2</sub><sup>2</sup>* parameter (Table S4) also explains the significant mixing of the higher-lying Kramers doublets. The principal reason for the magnetic

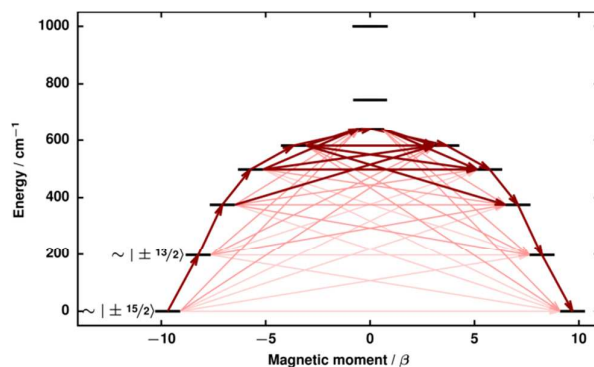


Fig. 4 Calculated magnetic relaxation barrier for **1<sub>Dy</sub>**. Darker arrows indicate the largest matrix elements, indicating the most probable relaxation route.

axiality in  $1_{\text{Dy}}$  is therefore the relatively large negative axial crystal field parameter  $B_2^0$ , whereas the other important axial parameters  $B_4^0$  and  $B_6^0$  are smaller.

In summary, the magnetic properties of the first pentalene-ligated SMM have been described. Large anisotropy barriers were determined for  $1_{\text{Dy}}$  and its magnetically dilute analogue, the origins of which were assigned to the strong axial field provided by the  $[\text{Cp}^*]^-$  ligand and the bridgehead carbon atoms of the  $[\text{Pn}^+]^{2-}$  ligand. The dominant relaxation process in  $1_{\text{Dy}}$  is thermally activated process via the second Kramers doublet. The appreciable equatorial field provided by the non-bridgehead carbon atoms attenuates the  $U_{\text{eff}}$  value and results in magnetic hysteresis occurring without coercivity. In terms of magneto-structural correlations, the folded nature of the pentalene ligand provides a unique coordination chemistry strategy for addressing the electronic structure of  $\text{Ln}^{3+}$  cations, and our on-going research will apply this in the design of magnetic, spintronic and optical materials.

The authors thank the European Research Council (AdG grant 247390, CoG grant 646740), the EPSRC (EP/M023885/1, EP/M022064/1), the Academy of Finland (projects 282499, 289172), Prof H. M. Tuononen (University of Jyväskylä) for providing computational resources, and Dr T. Pugh, Prof. R. N. Nair and Dr A. Achari (Manchester) for assistance with magnetic susceptibility measurements.

## Conflicts of interest

There are no conflicts to declare.

## Notes and references

- (a) S. K. Gupta and R. Murugavel, *Chem. Commun.*, 2018, **54**, 3685. (b) J. Lu, M. Guo and J. Tang, *Chem. Asian J.*, 2017, **12**, 2772. (c) J. M. Frost, K. L. M. Harriman and M. Murugesu, *Chem. Sci.*, 2016, **7**, 2470. (d) J.-L. Liu, Y.-C. Chen and M.-L. Tong, *Chem. Soc. Rev.*, 2018, **7**, 2431.
- S. Lumetti, A. Candini, C. Godfrin, F. Balestro, W. Wernsdorfer, S. Kiyatskaya, M. Ruben and M. Affente, *Dalton Trans.*, 2016, **45**, 16570.
- (a) C. Papatriantafyllopoulou, E. E. Moushi, G. Christou and A. J. Tasiopoulos, *Chem. Soc. Rev.*, 2016, **45**, 1597. (b) D. N. Woodruff, R. E. P. Winpenny and R. A. Layfield, *Chem. Rev.* 2013, **113**, 5110. (c) Y.-C. Chen, J.-L. Liu, L. Ungur, J. Liu, Q.-W. Li, L.-F. Wang, Z.-P. Ni, L. F. Chibotaru, X.-M. Chen and M.-L. Tong, *J. Am. Chem. Soc.*, 2016, **138**, 2829. (d) S. K. Gupta, T. Rajeshkumar, G. Rajaraman and R. Murugavel, *Chem. Sci.*, 2016, **7**, 5181. (e) T. Morita, M. Damjanovic, K. Katoh, Y. Kitagawa, N. Yasuda, Y. Lan, W. Wernsdorfer, B. K. Breedlove, M. Enders and M. Yamashita, *J. Am. Chem. Soc.*, 2018, **140**, 2995.
- R. A. Layfield, *Organometallics* 2014, **33**, 1084.
- (a) Y. Meng, Z. Mo, B. Wang, Y. Zhang, L. Deng and S. Gao, *Chem. Sci.*, 2015, **6**, 7156. (b) T. P. Latendresse, N. S. Bhuvanesh, M. Nippe, *J. Am. Chem. Soc.*, 2017, **139**, 14877.
- (a) R. A. Layfield, J. J. W. McDouall, S. A. Sulway, D. Collison, F. Tuna and R. E. P. Winpenny, *Chem. Eur. J.*, 2010, **16**, 4442. (b) T. Pugh, N. F. Chilton and R. A. Layfield, *Angew. Chem. Int. Ed.* 2016, **55**, 11082. (c) T. Pugh, F. Tuna, L. Ungur, D. Collison, E. J. L. McInnes, L. F. Chibotaru and R. A. Layfield, *Nat. Commun.* 2015, **6**, 7492. (d) T. Pugh, V. Vieru, L. F. Chibotaru and R. A. Layfield, *Chem. Sci.*, 2016, **7**, 2128. (e) T. Pugh, N. F. Chilton and R. A. Layfield, *Chem. Sci.*, 2017, **8**, 2073. (f) F.-S. Guo and R. A. Layfield, *Chem. Commun.*, 2017, **53**, 3130. (g) R. Grindell, B. M. Day, F.-S. Guo, T. Pugh and R. A. Layfield, *Chem. Commun.*, 2017, **53**, 9990.
- (a) F.-S. Guo, B. M. Day, Y.-C. Chen, M.-L. Tong, A. Mansikkamäki and R. A. Layfield, *Angew. Chem. Int. Ed.*, 2017, **56**, 11445. (b) S. Demir, M. I. Gonzalez, L. E. Darago, W. J. Evans and J. R. Long, *Nat. Commun.*, 2017, **8**, 2144. (c) S. Jiang, B. Wang, H. Sun, Z. Wang and S. Gao, *J. Am. Chem. Soc.*, 2011, **133**, 4730. (d) Y.-S. Meng, Y.-Q. Zhang, Z.-M. Wang, B.-W. Wang and S. Gao, *Chem. Eur. J.*, 2016, **22**, 12724. (e) C. A. P. Goodwin, F. Ortu, D. Reta, N. F. Chilton and D. P. Mills, *Nature*, 2017, **548**, 439. (f) C. P. Burns, B. O. Wilkins, C. M. Dickie, T. P. Latendresse, L. Vernier, K. R. Vignesh, N. S. Bhuvanesh and M. Nippe, *Chem. Commun.*, 2017, **53**, 8419.
- (a) L. Ungur, J. J. Le Roy, I. Korobkov and M. Murugesu, *Angew. Chem. Int. Ed.*, 2014, **53**, 4413. (b) J. J. Le Roy, L. Ungur, I. Korobkov, L. F. Chibotaru and M. Murugesu, *J. Am. Chem. Soc.*, 2014, **136**, 8003. (c) J. J. Le Roy, M. Jeletic, S. I. Gorelsky, I. Korobkov, L. Ungur, L. F. Chibotaru and M. Murugesu, *J. Am. Chem. Soc.*, 2013, **135**, 3502. (d) K. R. Meihaus and J. R. Long, *J. Am. Chem. Soc.*, 2013, **135**, 17952.
- K. L. M. Harriman, J. J. Le Roy, L. Ungur, R. Holmberg, I. Korobkov and M. Murugesu, *Chem. Sci.*, 2017, **8**, 231.
- F. G. N. Cloke, J. C. Green, A. F. R. Kilpatrick and D. O'Hare, *Coord. Chem. Rev.*, 2017, **344**, 238.
- (a) F. G. N. Cloke and P. B. Hitchcock, *J. Am. Chem. Soc.*, 2002, **124**, 9352. (b) A. E. Ashley, A. R. Cowley and D. O'Hare, *Eur. J. Org. Chem.*, 2007, 2239. (b) F. M. Chadwick and D. O'Hare, *Organometallics*, 2014, **133**, 3768.
- (a) A. F. R. Kilpatrick and F. G. N. Cloke, *Dalton Trans.*, 2017, **46**, 5587. (b) G. Balazs, F. G. N. Cloke, J. C. Green, R. M. Harker, A. Harrison, P. B. Hitchcock, C. N. Jardine and R. Walton, *Organometallics*, 2007, **26**, 3111.
- F. Aquilante, J. Autschbach, R. K. Carlson, L. F. Chibotaru, M. G. Delcey, L. De Vico, I. Fdez. Galván, N. Ferré, L. M. Frutos, L. Gagliardi, M. Garavelli, A. Giussani, C. E. Hoyer, G. Li Manni, H. Lischka, D. Ma, P. Å. Malmqvist, T. Müller, A. Nenov, M. Olivucci, T. B. Pedersen, D. Peng, F. Plasser, B. Pritchard, M. Reiher, I. Rivalta, I. Schapiro, J. Segarra-Martí, M. Stenrup, D. G. Truhlar, L. Ungur, A. Valentini, S. Vancollie, V. Veryazov, V. P. Vysotskiy, O. Weingart, F. Zapata and R. Lindh, *J. Comp. Chem.*, 2016, **37**, 506.
- L. Ungur and L. F. Chibotaru, *Chem. Eur. J.*, 2017, **23**, 3708.
- L. Ungur, M. Thewissen, J.-P. Costes, W. Wernsdorfer and L. F. Chibotaru, *Inorg. Chem.*, 2013, **52**, 6328.

## Electronic Supplementary Information

**Single-molecule magnet properties of a monometallic dysprosium pentalene complex**

Alexander F. R. Kilpatrick,<sup>a</sup> Fu-Sheng Guo,<sup>b</sup> Benjamin M. Day,<sup>b</sup>  
Akseli Mansikkamäki,<sup>\*c</sup> Richard A. Layfield<sup>\*a</sup> and F. Geoffrey N. Cloke<sup>\*a</sup>

<sup>a</sup>Department of Chemistry, School of Life Sciences, University of Sussex,  
Brighton, BN1 9QJ, UK.

<sup>b</sup>School of Chemistry, The University of Manchester, Manchester, M13 9PL, U.K.

<sup>c</sup>Department of Chemistry, Nanoscience Center, University of Jyväskylä,  
P.O. Box 35, Jyväskylä, FI-40014, Finland.

**Experimental: general considerations**

All manipulations were carried out using standard Schlenk techniques under argon, or in an MBraun glovebox under an inert atmosphere of nitrogen or argon. All glassware was dried at 160°C overnight prior to use. Solvents were purified by pre-drying over sodium wire and then distilled over Na (toluene), K (THF, hexane) or Na-K alloy (pentane) under nitrogen. Dried solvents were collected, degassed and stored over argon in K mirrored ampoules, except THF which was stored in ampoules containing activated 4 Å molecular sieves. Deuterated solvent (C<sub>6</sub>D<sub>6</sub>) was degassed by three freeze-pump-thaw cycles, dried by refluxing over potassium for three days, vacuum distilled into ampoules and stored under nitrogen. K<sub>2</sub>Pn<sup>†</sup> was prepared according to a published procedure.<sup>1</sup> DyCl<sub>3</sub> was prepared by dehydration of DyCl<sub>3</sub>·6H<sub>2</sub>O with excess Me<sub>3</sub>SiCl in refluxing heptane over three days. Anhydrous YCl<sub>3</sub> was kindly donated by co-workers.

NMR spectra were measured on Varian VNMRs 400 (<sup>1</sup>H 399.5 MHz; <sup>13</sup>C{<sup>1</sup>H} 100.25 MHz; <sup>29</sup>Si{<sup>1</sup>H} 79.4 MHz) or VNMRs 500 (<sup>1</sup>H 499.9 MHz; <sup>13</sup>C{<sup>1</sup>H} 125.7 MHz) spectrometers. The spectra were referenced internally to the residual protic solvent (<sup>1</sup>H) or the signals of the solvent (<sup>13</sup>C). <sup>29</sup>Si NMR spectra were referenced externally relative to SiMe<sub>4</sub>. Mass spectra were recorded by Dr A. Abdul-Sada at the University of Sussex using a VG Autospec Fisons instrument (electron ionisation at 70 eV). Elemental analyses for all compounds were carried out by Mr S. Boyer at the Elemental Analysis Service, London Metropolitan University.

Magnetic measurements were carried out using Quantum Design MPMS-7 or MPMP3 SQUID magnetometers at temperatures in the range 1.8-300 K. The samples were prepared in the glovebox by restraining a crystalline sample in eicosane, contained in an NMR tube sealed with a J. Young valve. The samples were then placed under vacuum and flame-sealed. Values of the magnetic susceptibility were corrected for the underlying diamagnetic increment by using tabulated Pascal constants, and the effect of the blank sample holders (gelatin capsule/straw).

Single crystal X-ray diffraction data for **1<sub>Dy</sub>** and **1<sub>Y</sub>** were collected on an Agilent Technologies Xcalibur Gemini Ultra diffractometer (CuKα source, λ = 1.54184 Å) equipped with a Eos CCD area detector. The data were collected at 173 K using an Oxford Cryosystems Cobra low temperature device. Data were processed using CrysAlisPro (version 1.171.36.32),<sup>2</sup> and unit cell parameters were refined against all data. An empirical absorption correction was carried out using the MULTI-SCAN program.<sup>3</sup> Structures were solved using DIRDIF-2008<sup>4</sup> or SUPERFLIP<sup>5</sup> and refined on Fo<sup>2</sup> by full-matrix least-squares refinements using SHELXL-2013.<sup>6</sup> Solutions and refinements were performed using the Olex2<sup>7</sup> or WinGX<sup>8</sup> packages and software packages within. All non-hydrogen atoms were refined with anisotropic displacement parameters. All hydrogen atoms parameters were constrained. For both **1<sub>Dy</sub>** and **1<sub>Y</sub>** the Cp\* ligand (C27 to C36) was positionally disordered over two sites. The disorder was modelled adequately by splitting the Me groups (C32 to C36) over two positions. For **1<sub>Dy</sub>**, restrain instructions were applied to give the thermal parameters more reasonable values, and the distance C31-C36A was restrained to prevent serious CheckCIF alerts.



### Synthesis of **1<sub>Dy</sub>**

A solution of  $\text{K}_2\text{Pn}^+$  (590 mg, 1.20 mmol) in THF (20 mL) was added dropwise to a suspension of  $\text{DyCl}_3$  (322 mg, 1.20 mmol) in THF (40 mL) and stirred for three hours. Solid  $\text{NaCp}^*$  (189 mg, 1.19 mmol) was added slowly and the resulting orange mixture was stirred at room temperature for 12 hours, then at  $75^\circ\text{C}$  for three hours. The solvent was removed *in vacuo* and the residues were extracted with hexane ( $3 \times 10$  mL) and filtered through Celite on a frit. The filtrate was stripped to dryness and the crude orange solids were recrystallised from pentane at  $-35^\circ\text{C}$ . Total yield: 290 mg (34% with respect to  $\text{K}_2\text{Pn}^+$ ). EI-MS:  $m/z = 712$  (100%),  $[\text{M}]^+$ ; 669 (25%),  $[\text{M} - ^i\text{Pr}]^+$ ; 577 (20%),  $[\text{M} - \text{Cp}^*]^+$ . Anal. found (calcd. for  $\text{C}_{36}\text{H}_{61}\text{DySi}_2$ ): C, 60.52 (60.68); H, 8.72 (9.62)%.

### Synthesis of **1<sub>Y</sub>**

Following a procedure analogous to the preparation of **1<sub>Dy</sub>**, starting from  $\text{YCl}_3$  (153 mg, 0.784 mmol) afforded **1<sub>Y</sub>** in 30% yield. X-ray quality crystals were grown from a saturated pentane-toluene solution (10:1 v/v) at  $-35^\circ\text{C}$ .  $^1\text{H}$  NMR ( $\text{C}_6\text{D}_6$ , 399.5 MHz, 303 K):  $\delta_{\text{H}}$  6.74 (2H, dd,  $J_{\text{YH}} = 1.1$ ,  $^3J_{\text{HH}} = 3.0$  Hz, Pn H), 5.40 (2H, d,  $^3J_{\text{HH}} = 3.1$  Hz, Pn H), 1.96 (15H, s,  $\text{Cp}^* \text{CH}_3$ ), 1.26 (6H, m,  $^i\text{Pr CH}$ ), 1.15 (18H, d,  $^3J_{\text{HH}} = 7.2$  Hz,  $^i\text{Pr CH}_3$ ), 1.03 (18H, d,  $^3J_{\text{HH}} = 7.3$  Hz,  $^i\text{Pr CH}_3$ ).  $^{13}\text{C}\{^1\text{H}\}$  NMR ( $\text{C}_6\text{D}_6$ , 125.7 MHz, 303 K):  $\delta_{\text{C}}$  147.1 (d,  $J_{\text{YC}} = 3.2$  Hz, Pn bridgehead C), 131.8 (d,  $J_{\text{YC}} = 1.4$  Hz, Pn CH), 119.5 (d,  $J_{\text{YC}} = 1.8$  Hz, Pn CH), 103.1 (s,  $\text{Cp}^* \text{CCH}_3$ ), 98.48 (d,  $J_{\text{YC}} = 1.7$  Hz, Pn C-Si), 19.68 (s,  $^i\text{Pr CH}_3$ ), 19.47 (s,  $^i\text{Pr CH}_3$ ), 12.76 (s,  $^i\text{Pr CH}$ ), 11.50 (s,  $\text{Cp}^* \text{CCH}_3$ ).  $^{29}\text{Si}\{^1\text{H}\}$  NMR ( $\text{C}_6\text{D}_6$ , 79.4 MHz, 303 K):  $\delta_{\text{Si}}$  1.98. EI-MS:  $m/z = 639$  (100%),  $[\text{M}]^+$ . Anal. found (calcd. for  $\text{C}_{36}\text{H}_{61}\text{Si}_2\text{Y}$ ): C, 67.51 (67.67); H, 9.58 (9.62) %.

### Synthesis of **Dy@1<sub>Y</sub>**

The magnetic site 20-fold diluted sample was synthesised by combination of the crude solids **1<sub>Y</sub>** and **1<sub>Dy</sub>** in a 20:1 molar ratio, followed by recrystallisation from pentane at  $-35^\circ\text{C}$ . Accurate dysprosium/yttrium ratios were measured by inductively coupled plasma atomic emission (ICP) spectroscopy using a Thermo iCap 6300 ICP-OES instrument, which resulted in a dysprosium content of  $5.0 \pm 0.5\%$ .

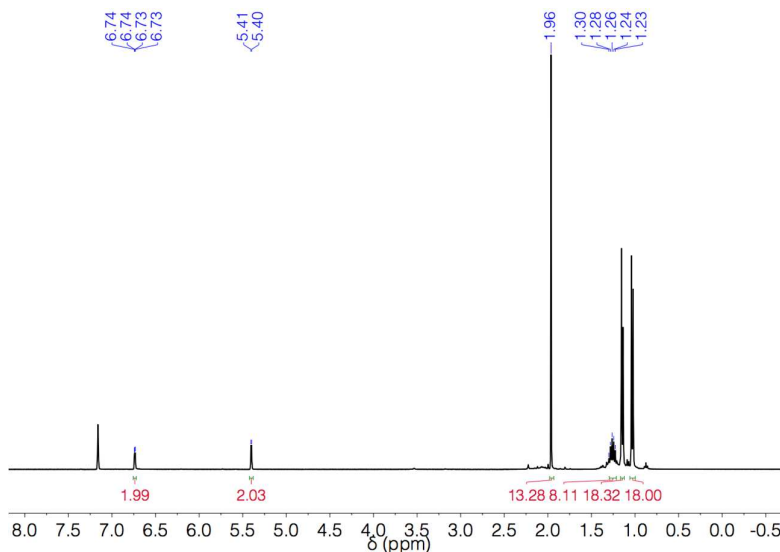


**Figure S1**  $^1\text{H}$  NMR spectrum ( $\text{C}_6\text{D}_6$ , 399.5 MHz, 303 K) of **1<sub>Y</sub>**.

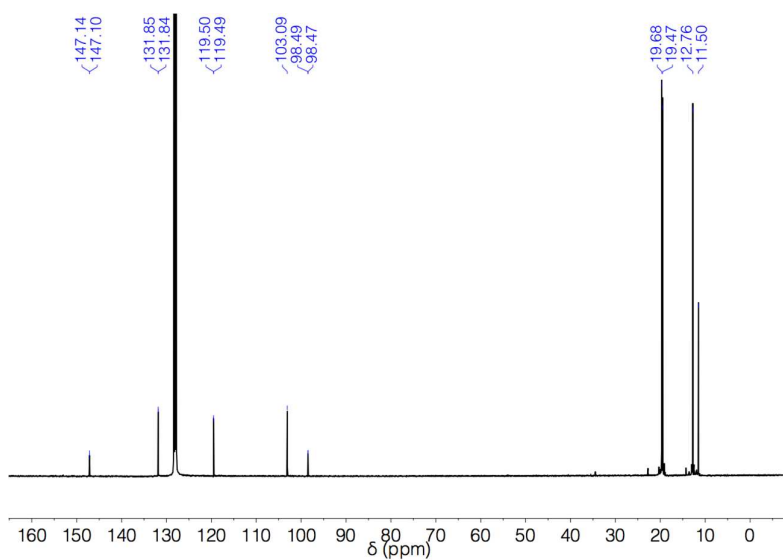


**Figure S2**  $^{13}\text{C}$  NMR spectrum (CD<sub>6</sub>, 125.7 MHz, 303 K) of **1<sub>Y</sub>**.

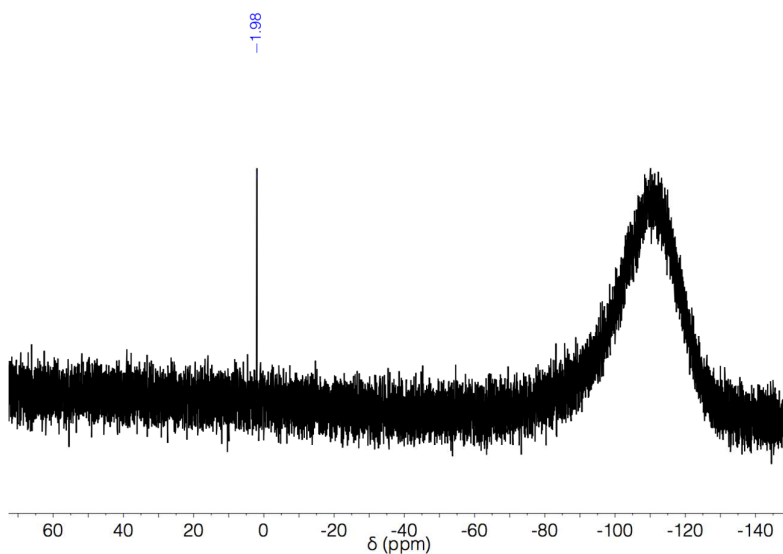


**Figure S3**  $^{29}\text{Si}$  NMR spectrum (CD<sub>6</sub>, 79.4 MHz, 303 K) of **1<sub>Y</sub>**.



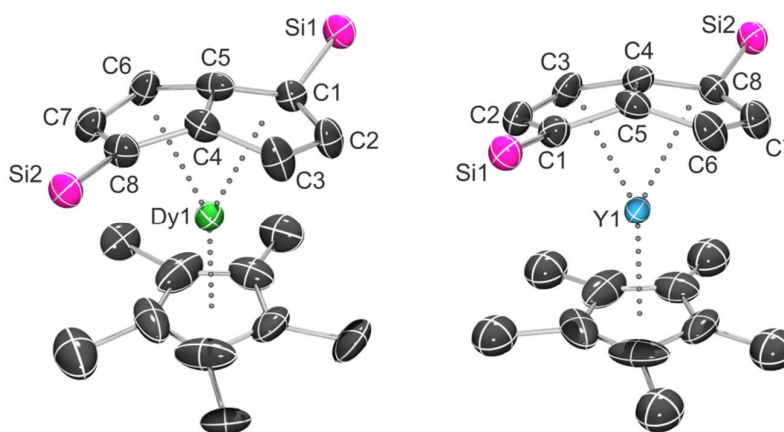


**Figure S4** Thermal displacement ellipsoid drawings (50% probability) of **1<sub>Dy</sub>** and **1<sub>Y</sub>**. Hydrogen atoms and <sup>i</sup>Pr groups mitted for clarity. One part of the disordered Cp\* methyl groups is omitted.

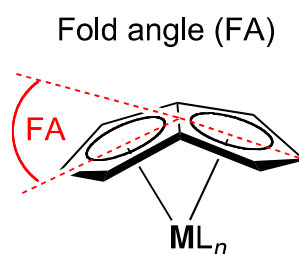


**Figure S5** The fold angle (FA) is defined as the dihedral angle between the two C<sub>5</sub> planes.

**Table S1** Selected distances (Å) and angles (°) for **1<sub>Dy</sub>** and **1<sub>Y</sub>**.

	<b>1<sub>Dy</sub></b>	<b>1<sub>Y</sub></b>
M–C(1)	2.621(6)	2.628(4)
M–C(2)	2.739(6)	2.736(4)
M–C(3)	2.606(7)	2.585(3)
M–C(4)	2.359(7)	2.357(3)
M–C(5)	2.371(7)	2.369(4)
M–C(6)	2.600(6)	2.603(4)
M–C(7)	2.731(6)	2.736(3)
M–C(8)	2.640(6)	2.620(3)
M–C(Cp*)	2.610(9)–2.643(12)	2.597(7)–2.634(7)
M–Pn <sub>cent</sub> (1)	2.235(3)	2.2295(16)
M–Pn <sub>cent</sub> (2)	2.235(3)	2.2283(18)
M–Cp <sub>cent</sub>	2.344(5)	2.334(3)
(C4–C5)–M–Cp <sub>cent</sub>	169.30(13)	171.06(9)
Fold angle	26.9(4)	27.0(2)

**Table S2** Selected experimental crystallographic data.

Structure	$1_{Dy}$	$1_Y$
<b>Crystal data</b>		
Chemical formula	$C_{36}H_{61}DySi_2$	$C_{36}H_{61}Si_2Y$
$M_r$	712.52	638.93
Crystal system, space group	triclinic, $P\bar{1}$	triclinic, $P\bar{1}$
$a, b, c$ (Å)	9.6968 (5), 12.7898 (6), 16.0392 (7)	9.7114(4), 12.7624(6), 15.9778(8)
$\alpha, \beta, \gamma$ (°)	71.948 (4), 75.157 (4), 80.771 (4)	72.103(4), 75.026(4), 80.722(4)
$V$ (Å <sup>3</sup> )	1821.05 (16)	1813.26(16)
$Z$	2	2
$\mu$ (mm <sup>-1</sup> )	11.74	3.04
Crystal size (mm)	$0.25 \times 0.20 \times 0.10$	$0.80 \times 0.70 \times 0.10$
<b>Data collection</b>		
$T_{min}, T_{max}$	0.378, 1.000	0.528, 1.000
No. of measured, independent and observed [ $I > 2\sigma(I)$ ] reflections	10563, 6300, 5484	10861, 6770, 6341
$R_{int}$	0.052	0.044
$(\sin \sigma/\lambda)_{max}$ (Å <sup>-1</sup> )	0.595	0.615
<b>Refinement</b>		
$R[F^2 > 2\sigma(F^2)], wR(F^2), S$	0.047, 0.113, 0.88	0.057, 0.154, 0.94
No. of reflections	6300	6770
No. of parameters	398	344
No. of restraints	61	0
$\Delta\rho_{max}, \Delta\rho_{min}$ (e Å <sup>-3</sup> )	0.78, -0.94	1.97, -1.10

For all structures: triclinic,  $P\bar{1}$ ,  $Z = 2$ . Experiments were carried out at 173 K with Cu  $K\alpha$  radiation using an Xcalibur, Eos, Gemini ultra. Absorption was corrected for by multi-scan methods, *CrysAlis PRO*, Agilent Technologies, Version 1.171.36.32 (release 02-08-2013 CrysAlis171 .NET) (compiled Aug 2 2013, 16:46:58) Empirical absorption correction using spherical harmonics, implemented in SCALE3 ABSPACK scaling algorithm. H-atom parameters were constrained.

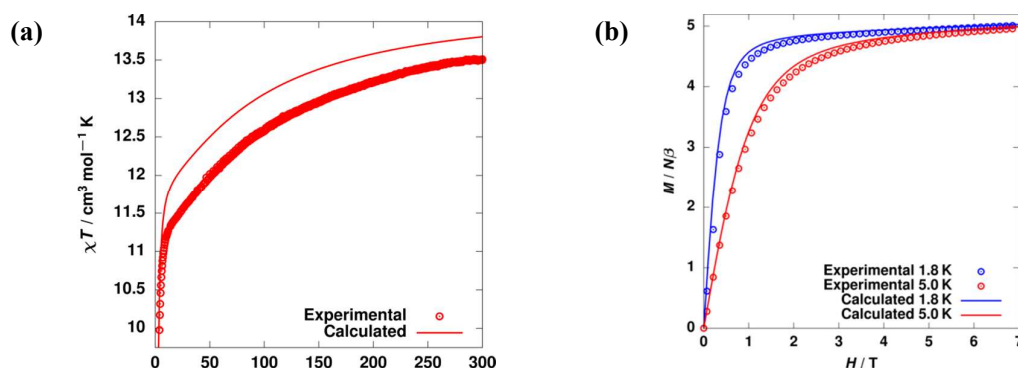


**Figure S6** (a) Temperature-dependent magnetic susceptibility acquired in a field of  $H_{dc} = 5000$  Oe; (b) field-dependent isothermal magnetization at 1.8 K and 5.0 K.

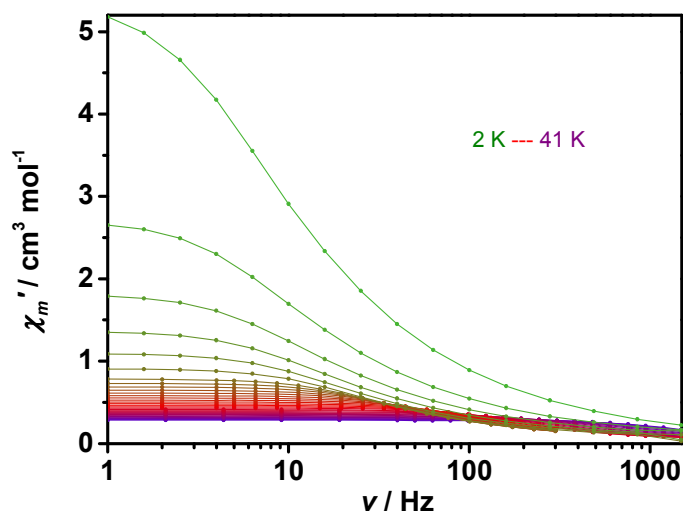


**Figure S7** Frequency dependence of the in-phase ( $\chi'$ ) AC susceptibility component in zero DC field at different temperatures for  $1_{Dy}$ . The solid lines are a guide for the eye.

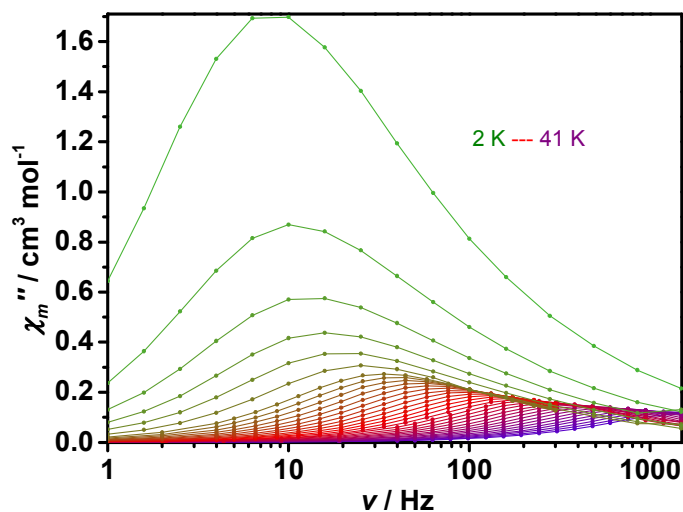


**Figure S8** Frequency dependence of the out of phase ( $\chi''$ ) AC susceptibility component in zero DC field at different temperature for  $1_{Dy}$ . The solid lines are a guide for the eye.

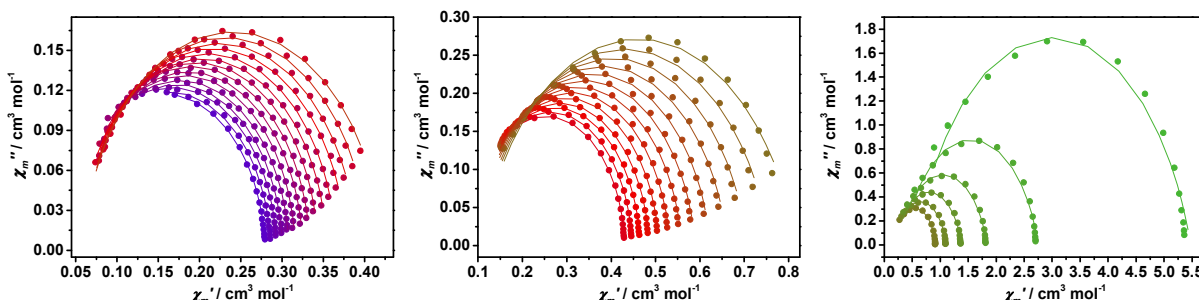


**Figure S9** Cole-Cole plot at  $T = 41-27$  K (left),  $T = 26-14$  K (centre) and  $T = 12-2$  K (right) using the AC susceptibility data for  $1_{Dy}$ . The solid lines are the best fits obtained with a generalized Debye model.

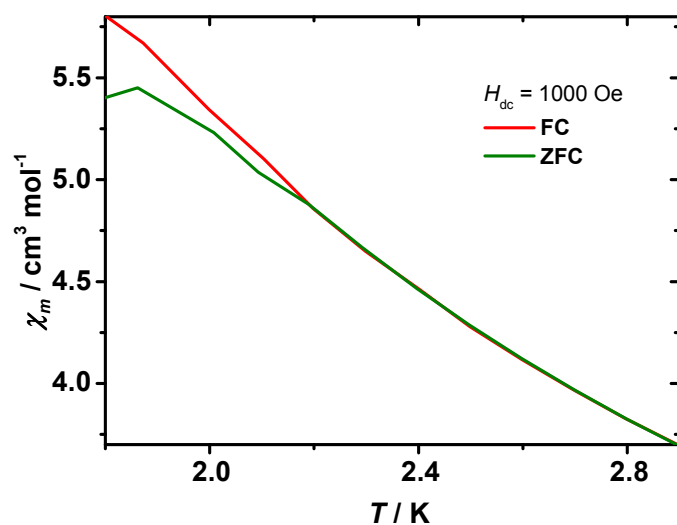


**Figure S10** Field-cooled (green) and zero-field-cooled (red) variable-temperature magnetic susceptibility for  $\text{Dy}$  at 1000 Oe in warming mode (2 K/min).

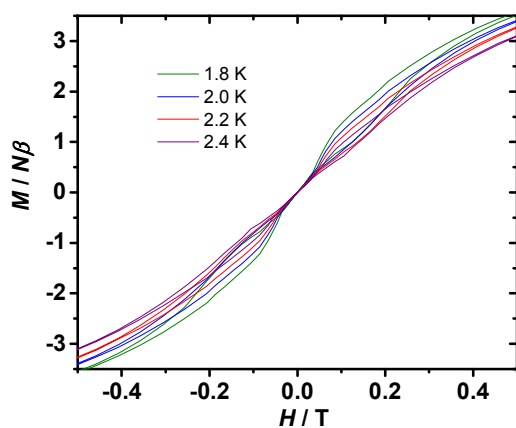


**Figure S11** Magnetization vs. field hysteresis for  $\text{Dy}$  under an average sweep rate of  $6.6 \text{ Oe s}^{-1}$ .

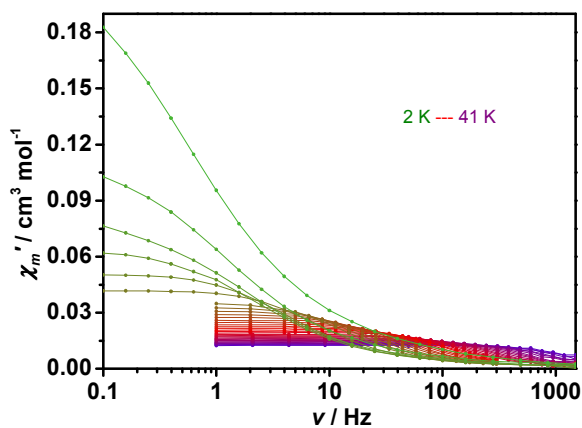


**Figure S12** Frequency dependence of the in-phase ( $\chi'$ ) AC susceptibility component in zero DC field at different temperatures for  $\text{Dy@1y}$ . The solid lines are a guide for the eye.

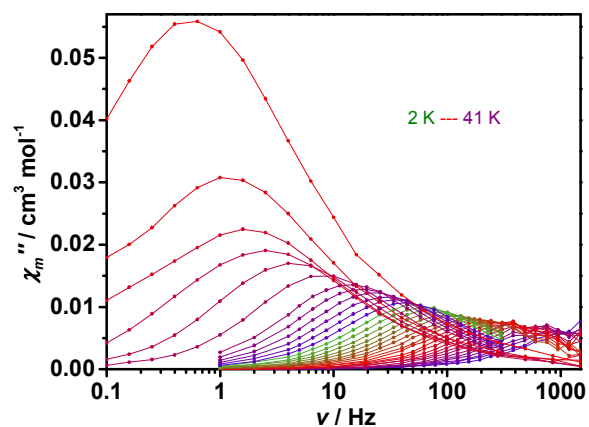


**Figure S13** Frequency dependence of the out of phase ( $\chi''$ ) AC susceptibility component in zero DC field at different temperature for  $\text{Dy@1Y}$ . The solid lines are a guide for the eye.

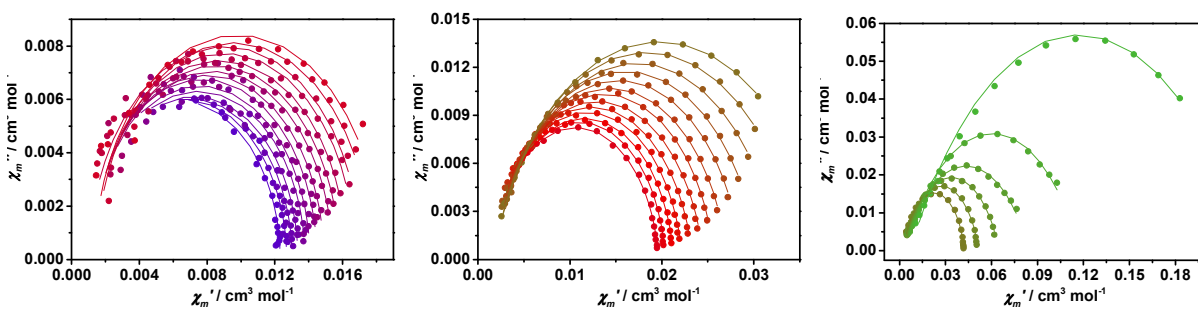


**Figure S14** Cole-Cole plot at  $T = 41\text{--}27\text{ K}$  (left),  $T = 26\text{--}14\text{ K}$  (centre) and  $T = 12\text{--}2\text{ K}$  (right) using the ac susceptibility data for  $\text{Dy@1Y}$ . The solid lines are the best fits obtained with a generalized Debye model.

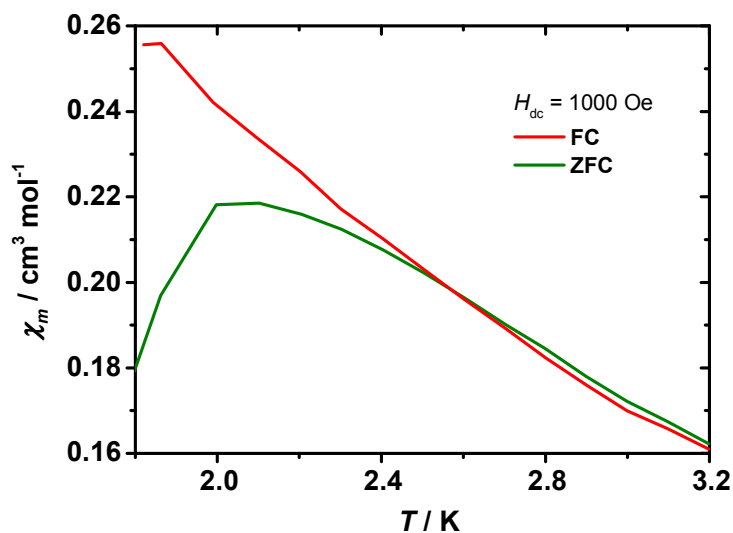


**Figure S15** Field cooled (FC, green) and zero-field-cooled (ZFC, red) variable-temperature magnetic susceptibility for  $\text{Dy@1Y}$  at 1000 Oe in warm mode (2 K/min).

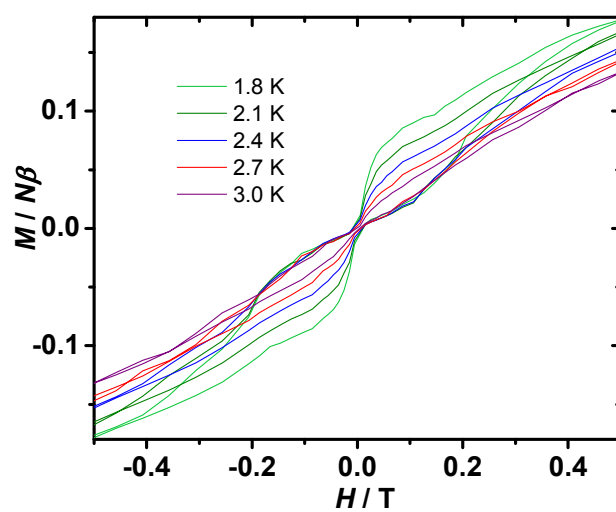


**Figure S16** Hysteresis for **Dy@1Y** under an average field sweep rate of  $9.8 \text{ Oe s}^{-1}$ .



### Computational Details

The geometry of **1<sub>Dy</sub>** was extracted from the crystal structure. Positions of hydrogen atoms were optimized at DFT level using the pure GGA PBE exchange correlation functional<sup>9</sup> while the positions of the heavier atoms were kept frozen to their respective crystal structure coordinates. The Dy<sup>3+</sup> ion was replaced by Y<sup>3+</sup> in the geometry optimizations to avoid convergence problems. Ahlrichs' def2-SVP basis sets were used in all DFT calculations. The core electrons of Y were treated with an effective core potential (ECP).<sup>10</sup> The DFT calculations were carried out using the Orca 4.0.0 code.<sup>11</sup>

The multi-reference *ab initio* calculations were performed using the standard CASSCF/SO-RASSI methodology as implemented in the Molcas quantum chemistry code versions 8.0 and 8.2.<sup>12</sup> Scalar relativistic effects were treated using the exact two component (X2C) transformation.<sup>13</sup> Roos' ANO-RCC basis sets were employed in all multireference calculations. A VQZP quality basis set corresponding to a [9s8p6d4f3g2h] contraction was used for Dy<sup>3+</sup>, VTZP basis sets corresponding to [4s3p2d1f] and [3s2p1d] contractions were used for the C and H atoms in the cyclopentadienyl and pentalene cores, respectively, and VDZP quality basis sets corresponding to [4s3p1d], [3s2p1d], and [2s1p] contractions were used for the Si, and other C and H atoms, respectively.<sup>14</sup> A state-averaged CASSCF calculation<sup>15</sup> correlating all nine 4f electrons in the seven 4f orbitals was performed. All 21 sextets, 224 doublets, and 490 doublets were solved. The lowest 21 sextets, 128 quartets, and 130 doublets (corresponding to an energy cut-off of 50,000 cm<sup>-1</sup>) were mixed by spin-orbit coupling using the restricted active space state interaction (SO-RASSI) method.<sup>16</sup> All spin 21 spin-sextets were included in the SO-RASSI procedure. The local magnetic properties (**g** tensor, crystal field parameters, magnetic susceptibility, magnetization, and transition magnetic moments) were then extracted from the SO-RASSI wave functions using the SINGLE\_ANISO routine.<sup>17-19</sup>

**Table S3** Properties of the eight lowest Kramers' doublets in the ground <sup>6</sup>H<sub>15/2</sub> multiplet of **1<sub>Dy</sub>**.

KD	<i>E</i> / cm <sup>-1</sup>	<i>g<sub>x</sub></i>	<i>g<sub>y</sub></i>	<i>g<sub>z</sub></i>	θ <sup>a</sup>
1	0	0.0024	0.0040	19.3900	
2	197	0.0251	0.0277	16.5060	4.0°
3	375	0.1234	0.1492	14.1861	3.3°
4	498	0.5948	0.7648	11.4585	1.1°
5	581	4.1225	4.2798	7.6541	16.4°
6	642	2.6966	5.0779	10.9892	90.7°
7	744	0.2216	0.4375	16.5020	91.5°
8	1000	0.0042	0.0081	19.8478	88.6°

<sup>a</sup> The angle between the principal axis of the doublet and the principal axis of the ground doublet.

**Table S4** *Ab initio* calculated crystal-field parameters for **1<sub>Dy</sub>**.

<i>k</i>	<i>q</i>	<i>B(k,q)</i>
2	− 2	−0.297232
2	− 1	0.208131
2	0	−4.588615
2	1	0.483546
2	2	3.894423
4	− 4	−0.000472
4	− 3	−0.001782
4	− 2	0.001115
4	− 1	−0.001247
4	0	0.001066
4	1	−0.003708
4	2	0.007971
4	3	−0.000507
4	4	0.007354
6	− 6	−0.000007
6	− 5	0.000039
6	− 4	0.000011
6	− 3	−0.000012
6	− 2	0.000024
6	− 1	−0.000013
6	0	−0.000014
6	1	−0.000076
6	2	0.000221
6	3	−0.000252
6	4	−0.000171
6	5	0.000379
6	6	0.000052

**Table S5** Squared projections of the 16 lowest states (belonging to the eight lowest KDs) of  $1D_y$  onto  $|JM_J\rangle$  states where  $J = 15/2$ .

	KD1		KD2		KD3		KD4		KD5		KD6		KD7		KD8	
$M_J = -15/2$	0.925	0.000	0.001	0.000	0.000	0.000	0.072	0.000	0.001	0.001	0.000	0.000	0.000	0.000	0.000	0.000
$M_J = -13/2$	0.001	0.000	0.888	0.000	0.000	0.000	0.002	0.000	0.105	0.000	0.000	0.000	0.002	0.000	0.000	0.000
$M_J = -11/2$	0.068	0.000	0.001	0.000	0.000	0.000	0.808	0.000	0.006	0.101	0.000	0.007	0.002	0.004	0.001	0.001
$M_J = -9/2$	0.002	0.000	0.099	0.000	0.000	0.000	0.007	0.000	0.731	0.004	0.010	0.014	0.091	0.002	0.032	0.005
$M_J = -7/2$	0.004	0.000	0.003	0.000	0.000	0.000	0.098	0.000	0.011	0.560	0.004	0.116	0.017	0.137	0.011	0.034
$M_J = -5/2$	0.000	0.000	0.007	0.000	0.000	0.000	0.001	0.000	0.129	0.003	0.006	0.036	0.340	0.029	0.313	0.057
$M_J = -3/2$	0.000	0.000	0.000	0.000	0.000	0.000	0.010	0.001	0.000	0.247	0.001	0.027	0.001	0.380	0.012	0.223
$M_J = -1/2$	0.000	0.000	0.000	0.000	0.000	0.000	0.001	0.000	0.015	0.003	0.059	0.025	0.321	0.005	0.075	0.160
$M_J = 1/2$	0.000	0.000	0.000	0.000	0.001	0.000	0.015	0.000	0.059	0.003	0.321	0.025	0.075	0.005	0.336	0.160
$M_J = 3/2$	0.000	0.000	0.000	0.000	0.010	0.000	0.000	0.001	0.001	0.247	0.001	0.027	0.012	0.380	0.098	0.223
$M_J = 5/2$	0.000	0.000	0.000	0.007	0.001	0.000	0.129	0.000	0.006	0.003	0.340	0.036	0.313	0.029	0.079	0.057
$M_J = 7/2$	0.000	0.004	0.000	0.003	0.098	0.000	0.011	0.000	0.004	0.560	0.017	0.116	0.011	0.137	0.004	0.034
$M_J = 9/2$	0.000	0.002	0.000	0.099	0.007	0.000	0.731	0.000	0.010	0.004	0.091	0.014	0.032	0.002	0.002	0.005
$M_J = 11/2$	0.000	0.068	0.000	0.001	0.808	0.000	0.006	0.000	0.000	0.101	0.002	0.007	0.001	0.004	0.000	0.001
$M_J = 13/2$	0.000	0.001	0.000	0.888	0.002	0.000	0.105	0.000	0.000	0.000	0.002	0.000	0.000	0.000	0.000	0.000
$M_J = 15/2$	0.000	0.925	0.000	0.001	0.072	0.000	0.001	0.000	0.000	0.001	0.000	0.000	0.000	0.000	0.000	0.000

## References

1. F. G. N. Cloke, M. C. Kuchta, R. M. Harker, P. B. Hitchcock and J. S. Parry, *Organometallics*, 2000, **19**, 5795.
2. Agilent Technologies, *CrysAlisPro 1.171.36.32*, 2011.X
3. (a) R. H. Blessing and D. A. Langa, *J. Appl. Crystallogr.*, 1987, **20**, 427. (b) R. H. Blessing, *Acta Crystallogr., A, Found. Crystallogr.*, 1995, **51**, 33.
4. P. T. Beurskens, G. Beurskens, R. Gelder, J. M. M. Smits, S. de Garcia-Granda, and R. O. Gould, 2008. The *DIRDIF2008* program system, Crystallography Laboratory, University of Nijmegen, The Netherlands.
5. L. Palatinus and G. Chapuis, *J. Appl. Crystallogr.*, 2007, **40**, 786.
6. G. M. Sheldrick, *Acta Crystallogr., A*, 2008, **64**, 112.
7. O. V. Dolomanov, L. J. Bourhis, R. J. Gildea, J. A. K. Howard and H. Puschmann, *J. Appl. Crystallogr.*, 2009, **42**, 339.
8. O. V. Dolomanov, L. J. Bourhis, R. J. Gildea, J. A. K. Howard and H. Puschmann, *J. Appl. Crystallogr.*, 2009, **42**, 339.
9. (a) J. P. Perdew, K. Burke, M. Ernzerhof. *Phys. Rev. Lett.*, **1996**, **77**, 3865; (b) J. P. Perdew, K. Burke, M. Ernzerhof. *Phys. Rev. Lett.*, 1996, **78**, 1396.
10. (a) F. Weigend, R. Ahlrichs. *Phys. Chem. Chem. Phys.*, 2005, **7**, 3297; (b) A. Schäfer, H. Horn, R. Ahlrichs. *J. Chem. Phys.*, 1992, **97**, 2571.
11. F. Neese. *WIREs Comput. Mol. Sci.*, 2017, **8**, e1327.
12. F. Aquilante, J. Autschbach, R. K. Carlson, L. F. Chibotaru, M. G. Delcey, L. De Vico, I. Fdez. Galván, N. Ferré, L. M. Frutos, L. Gagliardi, M. Garavelli, A. Giussani, C. E. Hoyer, G. Li Manni, H. Lischka, D. Ma, P. Å. Malmqvist, T. Müller, A. Nenov, M. Olivucci, T. B. Pedersen, D. Peng, F. Plasser, B. Pritchard, M. Reiher, I. Rivalta, I. Schapiro, J. Segarra-Martí, M. Stenrup, D. G. Truhlar, L. Ungur, A. Valentini, S. Vancoillie, V. Veryazov, V. P. Vysotskiy, O. Weingart, F. Zapata, R. Lindh, *J. Comp. Chem.*, 2016, **37**, 506.
13. (a) W. Kutzelnigg, W. Liu. *J. Chem. Phys.*, 2005, **123**, 241102; (b) P. Daoling, M. Reiher. *Theor. Chem. Acc.*, 2012, **131**, 1.
14. (a) K. Andersson, P. Å. Malmqvist, B. O. Roos. *J. Chem. Phys.*, **1992**, **96**, 1218; (b) B. O. Roos, R. Lindh, P. Å. Malmqvist, V. Veryazov, P.-O. Widmark. *J. Phys. Chem. A*, **2004**, **108**, 2851; (c) B. O. Roos, R. Lindh, P. Å. Malmqvist, V. Veryazov, P.-O. Widmark, A. C. Borin. *J. Chem. Phys. A*, 2008, **112**, 11431.
15. (a) B. O. Roos in *Advances in Chemical Physics, Ab Initio Methods in Quantum Chemistry II*, Vol. 69 (Ed.: K. P. Lawley), Wiley, New York, 1987, pp. 399–455. (b) B. O. Roos, R. Lindh, P. Å. Malmqvist, V. Veryazov, P.-O. Widmark. *Multiconfigurational Quantum Chemistry*. Wiley, Hoboken, NJ, 2016.
16. P. Å. Malmqvist, B. O. Roos, B. Schimmelpfennig. *Chem. Phys. Lett.*, 2002, **357**, 230.
17. (a) L. F. Chibotaru, L. Ungur. *J. Chem. Phys.*, 2012, **137**, 064112. (b) L. Ungur, L. F. Chibotaru in *Lanthanides and Actinides in Molecular Magnetism. Computational Modelling of the Magnetic Properties of Lanthanide Compounds*. (Ed.: R. A. Layfield, M. Murugesu), Wiley-VHC, Weinheim, Germany, 2015, pp. 153-184.
18. L. Ungur, L. F. Chibotaru. *Chem. Eur. J.*, 2017, **23**, 3708.
19. L. Ungur, M. Thewissen, J.-P. Costes, W. Wernsdorfer, L. F. Chibotaru. *Inorg. Chem.*, 2013, **52**, 6328.